Observation of Photoinduced Charge Transfer in Novel Luminescent CdSe Quantum Dot−CePO4:Tb Metal Oxide Nanowire Composite Heterostructures

ARTICLE *in* THE JOURNAL OF PHYSICAL CHEMISTRY C · MARCH 2014

Impact Factor: 4.77 · DOI: 10.1021/jp4113816

3 AUTHORS, INCLUDING:

Jinkyu Han
Brookhaven National Laboratory
16 PUBLICATIONS **12** CITATIONS
SEE PROFILE

Lei Wang
Stony Brook University
14 PUBLICATIONS **43** CITATIONS
SEE PROFILE

THE JOURNAL OF PHYSICAL CHEMISTRY C

Article

pubs.acs.org/JPCC

Observation of Photoinduced Charge Transfer in Novel Luminescent CdSe Quantum Dot−$CePO_4$:Tb Metal Oxide Nanowire Composite Heterostructures

Jinkyu Han,[†] Lei Wang,[‡] and Stanislaus S. Wong*[,†,‡]

[†]Condensed Matter Physics and Materials Sciences Department, Building 480, Brookhaven National Laboratory, Upton, New York 11973, United States

[‡]Department of Chemistry, State University at New York at Stony Brook, Stony Brook, New York 11794-3400, United States

Supporting Information

ABSTRACT: We report on the synthesis, structural characterization, and intrinsic charge transfer processes associated with novel luminescent zero-dimensional (0D) CdSe nanocrystal−one-dimensional (1D) $CePO_4$:Tb nanowire composite heterostructures. Specifically, ∼4 nm CdSe quantum dots (QDs) have been successfully anchored onto high-aspect ratio $CePO_4$:Tb nanowires, measuring ∼65 nm in diameter and ∼2 μm in length. Composite formation was confirmed by high-resolution transmission microscopy, energy-dispersive X-ray spectroscopy mapping, and confocal microscopy. Photoluminescence (PL) spectra, emission decay, and optical absorption of these nanoscale heterostructures were collected and compared with those of single, discrete CdSe QDs and $CePO_4$:Tb nanowires. We show that our composite heterostructure evinces both PL quenching and a shorter average lifetime as compared with unbound CdSe QDs and $CePO_4$:Tb nanowires. We propose that a photoinduced 0D−1D charge transfer process occurs between CdSe and $CePO_4$:Tb and that it represents the predominant mechanism, accounting for the observed PL quenching and shorter lifetimes noted in our composite heterostructures. Data are additionally explained in the context of the inherent energy level alignments of both CdSe QDs and $CePO_4$:Tb nanowires.

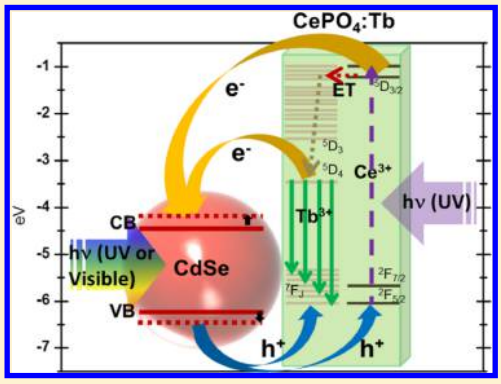

INTRODUCTION

Nanomaterials, including zero-dimensional (0D) and one-dimensional (1D) nanostructures, such as crystals, cubes, wires, rods, and tubes, have been extensively investigated due to their unique properties and potential usage in applications, including but not limited to catalysis, chemical sensing, microelectronics, and photovoltaics.[1] Recently, nanoscale heterostructures composed of different, distinctive, and complementary constituent subunits have become the focus of particular interest, because their unique multifunctional properties can potentially be tuned and tailored so as to render significant improvement and performance enhancement as compared with single-component systems. The idea is that the whole is often more interesting than the sum of its individual parts. In this light, as practical examples, extensive research has focused on creating novel semiconducting quantum dot (QD)−TiO_2 nanocrystal heterostructures, as well as TiO_2/ZnO nanotube−carbon nanotube (CNT) coupled architectures in order to improve the charge separation and transport capabilities for solar cell applications.[2−6] Moreover, work on both CuO/Si nanoparticle−CNT composites and SnO_2−α-Fe_2O_3 core−shell heterostructures has given rise to the potential and expectation for improved cycling performance and lithium ion storage capacities for Li-ion battery anode materials.[7,8]

More recently, this idea has been extended to the development of nanoscale rare earth doped inorganic composite luminescent materials, such as CdSe QD−$NaYF_4$:Yb, Er nanocrystals and CdS−$LaPO_4$:Eu^{3+} core−shell nanotubes.[9,10] In the first system based on 0D materials, the photoluminescence (PL) output of CdSe QDs and $NaYF_4$:Yb, Er nanocrystals could be enhanced through energy transfer from $NaYF_4$:Yb, Er nanocrystals to CdSe QDs excited at 980 nm, which is in the low-energy, near-infrared region. For the second example associated with 1D structural motifs, energy transfer from CdS to $LaPO_4$:Eu^{3+} has been observed upon excitation at 380 nm. Both of these examples highlight the synthetic potential to tune and properly design the optical properties of nanomaterials through the controlled formation of nanoscale heterostructures.

Hence, although some progress has been made in devising and fabricating nanoscale heterostructures as novel inorganic luminescent materials, reports on more sophisticated nanoscale architectures, composed of different, mixed morphologies such as 0D−1D composites, are few and far between, despite the

Received: November 19, 2013
Revised: February 5, 2014
Published: March 6, 2014

   dx.doi.org/10.1021/jp4113816 | J. Phys. Chem. C 2014, 118, 5671−5682

obvious and crucial role of nanostructure morphology in dictating their optical and electronic properties.[11−14] Therefore, herein, we aim to create a new 0D−1D heterostructure where we have purposely combined and interwoven both CdSe QDs nanocrystals (with their size-dependent absorption properties) and $CePO_4$:Tb nanowires (with their chemically defined PL attributes) into a highly efficient, discrete luminescent structure.

Years of prior research have extensively focused on the use of individual CdX, PbX, and ZnX (with X = Se, S, and Te) QDs as effective luminescent materials due to their potential applicability in color displays, light emitting diodes, medical and biological labels, as well as photovoltaic devices.[5,6,15−17] Yet, at the same time, a significant amount of equally relevant, perhaps less high-profile research has been devoted to the study of lanthanide-doped lanthanide orthophosphates, due to their lower photobleaching capability, comparatively high quantum yields (up to 60%), good chemical stability, and relatively low toxicity.[18,19] Specifically, Tb-doped $CePO_4$ nanostructures have been extensively used as a green emitting material in fluorescent lamps, and have also been considered for optoelectronics as well as for biological labeling applications.[20−22] In particular, the strong green emission of the Tb ions can be observed after UV excitation of Ce ions in the spectral range of 270−280 nm. To date, various lanthanide orthophosphates possessing different morphologies, such as 0D nanocrystals, 1D nanotubes, core/shell structures, and 3D sea urchin structures, have been successfully synthesized by using a number of different methods, including sol−gel, coprecipitation, hydrothermal, electrospinning, and microemulsion protocols.[23−27] Moreover, our group has developed a modified template technique, enabling us to prepare crystalline 1D nanostructures associated with classes of diverse materials.[28−31] Specifically, we have successfully prepared high-aspect-ratio, single-crystalline Tb-doped $CePO_4$ nanowires using a solution-based U-tube protocol.[20] Our methodology is run under ambient conditions, minimizes the use of either pyrophoric, flammable, or unstable precursors, maximizes yield, and can occur in as few steps as possible in aqueous solvents with little if any byproducts, giving rise to crystalline, reasonably pure nanomaterials.

Herein, we report the first synthetic demonstration and optical characterization of a model 0D quantum dot−1D metal oxide architecture. Specifically, we have prepared 0D CdSe QD−1D $CePO_4$:Tb nanowire heterostructures, wherein CdSe QDs have been successfully attached onto the external sidewalls of high aspect-ratio, green-emitting $CePO_4$:Tb nanowires. In particular, we have characterized the optical absorption, luminescence, and lifetimes of CdSe−$CePO_4$:Tb nanoscale heterostructures. In so doing, we have observed PL quenching and a shorter average lifetime of our modified, customized heterostructures as compared with unbound CdSe QDs and $CePO_4$:Tb nanowires. Moreover, the effect of varying the concentration ratios of CdSe QDs and $CePO_4$:Tb on the resulting PL quenching and lifetime of the resulting heterostructures has also been systematically examined. We propose that the observed PL quenching and the shorter average lifetimes of heterostructures can be directly attributed to the photoinduced charge transfer between the CdSe QDs and the $CePO_4$:Tb nanowires. Indeed, our inorganic luminescent semiconducting QD−$CePO_4$:Tb heterostructures represent an interesting structural paradigm for novel optoelectronic device applications. Specifically, these results may lead to distinctive designs for novel photovoltaic architectures with the capability of harvesting UV light as well as for promoting highly efficient charge separation.

EXPERIMENTAL SECTION

1. Synthesis. CdSe QDs have been prepared according to a well known, reasonably mild protocol, previously described.[32] In brief, 0.2 mmol of CdO and 0.8 mmol of stearic acid were degassed at 150 °C, and then heated under an Ar atmosphere to completely dissolve the precursors in a three-necked flask. Subsequently, trioctylphosphine oxide (TOPO) and hexadecylamine (HDA) (3.88 g of each) were added to the flask, and the mixture was heated to 320 °C. Two millimoles of selenium dissolved in tributylphosphine and dioctylamine was injected into the hot precursor solution at 320 °C, and subsequent growth was carried out at 270 °C for 3 min. The mixture was then allowed to cool to room temperature, and it was washed with a mixture of methanol or acetone, prior to dissolution in chloroform. 2-Aminoethanethiol (AET) capped CdSe QDs were obtained through a ligand exchange reaction. In a typical experiment, a solution of AET (0.1 mmol) in 2 mL of methanol was added to a suspension of as-prepared, capped CdSe QDs (0.04 mmol) in 4 mL of chloroform. After the mixture was stirred for 10 min, QDs were then precipitated upon ligand exchange. These QDs were later collected by centrifugation and subsequently washed with ethanol and methanol. The resulting QDs were finally redispersed in methanol for future use.

A typical synthesis of $CePO_4$:Tb nanowires was performed following our recently reported methods.[20] In a standard ambient protocol, polycarbonate track-etched membranes, containing pore sizes of 50-nm diameter, were initially hydrated by immersion and sonication, and then mounted between the two half arms of a U-shaped tube. One of the two half-cells was filled with a 0.01 M NaH_2PO_4 solution, which was adjusted to acidic reaction conditions (i.e., pH 3) by using dilute HCl, while the other half-cell contained a solution generated by mixing a 0.05 M $CeCl_3$ solution together with $Tb(NO_3)_3$ up to a final molar concentration of 5.0%, so as to generate the desired Tb-doped $CePO_4$ nanostructures. The aqueous solutions within the two half cells of the system were then allowed to diffuse toward each other in an unperturbed manner for an incubation period of 2 h at room temperature. The schematic of the U-tube protocol for the synthesis of $CePO_4$:Tb is shown in the Supporting Information, Figure S1. To isolate products within the template pores themselves, the polycarbonate membrane was detached, sonicated for about 2 min to remove the unwanted particles on the external surface, and thoroughly washed with distilled water, before being ultimately dissolved with methylene chloride. As-prepared, hydrated phosphate nanowires were later isolated from solution by centrifugation upon washing, and then stored in methanol.

TOPO and HDA capped CdSe QDs (i.e., as-prepared QDs) and AET capped CdSe QDs were attached onto $CePO_4$:Tb nanowires presumably through a hydrogen bonding mechanism involving water molecules intercalated in the $CePO_4$:Tb nanowire structure. In a typical experiment, 1.2 mg (5.2 μmol) of $CePO_4$:Tb in 2 mL of methanol was added to 1 mg (5.2 μmol) of as-prepared CdSe QDs (or AET-capped CdSe) in 2 mL of chloroform (or methanol). The resulting solution was subsequently sonicated for 10 min and stirred in the dark for 2 h.

2. Characterization. Samples were thoroughly characterized by using a number of different complementary methodologies, including powder X-ray diffraction (XRD), Fourier

dx.doi.org/10.1021/jp4113816 | J. Phys. Chem. C 2014, 118, 5671−5682

transform infrared spectroscopy (FTIR), transmission electron microscopy (TEM), energy-dispersive X-ray spectroscopy (EDS), high-resolution TEM (HRTEM), confocal microscopy (CFM), as well as UV−visible, steady-state photoluminescence (PL) spectroscopy, and time-resolved fluorescence lifetime spectroscopy.

2.1. X-ray Diffraction. Crystallographic and purity data on the CdSe QDs and $CePO_4$:Tb nanowires were initially obtained by using powder X-ray diffraction. To prepare the relevant samples, the resulting QDs and nanowire samples were rendered into slurries, i.e., in chloroform for QDs and in ethanol for $CePO_4$:Tb nanowires, respectively. Samples were sonicated for about 1 min, and then air-dried upon deposition onto glass slides. Diffraction patterns were subsequently collected with a Scintag diffractometer, operating in the Bragg configuration using Cu Kα radiation (1.54 Å), ranging from 20° to 80° at a scanning rate of 2° per minute.

2.2. Electron Microscopy. Low-magnification TEM images were taken at an accelerating voltage of 120 kV on a JEOL JEM-1400 instrument, equipped with EDS mapping capabilities. High-resolution TEM (HRTEM) images coupled with the ability to obtain selected area electron diffraction (SAED) patterns were recorded with a JEOL JEM-3000F microscope equipped with a Gatan image filter (GIF) spectrometer operating at an accelerating voltage of 300 kV. Specimens for all of these TEM experiments were prepared by dispersing the as-prepared product in ethanol, sonicating for 2 min to ensure an adequate dispersion of the nanostructures, and dipping one drop of the solution onto a 300 mesh Cu grid, coated with a lacey carbon film. Our statistical size measurements were obtained on 30 to 50 different nanostructures per sample analyzed.

2.3. FTIR. FTIR spectra were obtained on a Nexus 670 (ThermoNicolet) equipped with a Smart Orbit diamond ATR accessory, a KBr beam splitter, and a DTGS KBr detector. As-prepared solid powder samples were placed onto the crystal surface, where data were taken with a reproducible pressure. A background correction in air was performed in the spectral range studied. FTIR data were recorded typically over the wavenumber range of 1000−4000 cm^{-1} and evaluated in terms of expected, characteristic absorption bands. The spectra were recorded with the Omnic software at a spatial resolution of 1 cm^{-1}.

2.4. UV−Visible and Fluorescence Spectroscopy. UV−visible spectra were collected at high resolution on a Thermospectronics UV1 spectrometer, using quartz cells possessing a 10-mm path length. Spectra were obtained for CdSe QDs, $CePO_4$:Tb nanowires, and associated heterostructures, all of which were individually sonicated for 2 min so as to yield a homogeneous dispersion. Samples for PL spectra were dispersed in mixtures of chloroform and methanol for as-prepared CdSe QDs and CdSe QD−$CePO_4$:Tb heterostructures as well as in methanol itself for AET-capped CdSe QDs and their heterostructured composites with $CePO_4$:Tb nanowires. All were sonicated for 1 min prior to measurement. Fluorescence data were subsequently obtained at room temperature on a FluoroMax-4 spectrofluorimeter (Jobin Yvon) with 15 and 5 s integration times, using excitation wavelengths of 280 and 375 nm, respectively. The fluorescence lifetimes were measured by a FluoroMax-4 spectrofluorimeter with an IBH NanoLED, emitting at 388 nm as an excitation source, with a NanoLED controller module, Fluorohub (Jobin Yvon), operating at 1 MHz. Decay data analysis was performed with the DAS6 software (Horiba Jobin Yvon IBH).

2.4. Confocal Microscopy Imaging. Fluorescence images were taken by using a confocal fluorescence microscope (Leica, TCS SP5), equipped with an argon ion laser. Samples were subsequently excited under 455-nm irradiation, and images were separately collected via one-output channels, which were then monitored in the range of 550−600 nm. Acquired data were then analyzed by using the LSM 510 META software.

RESULTS AND DISCUSSION

1. Structural Insights into CdSe QDs and $CePO_4$:Tb Nanowires. We note that the XRD patterns of as-prepared CdSe QDs can be reliably assigned to the reflection of a crystalline hexagonal würzite structure (JCPDS No. 08-0459), as shown in Figure S2 in the Supporting Information. The corresponding purity and crystallinity of $CePO_4$:Tb nanowires, prepared by a U-tube template mediated synthesis, were initially characterized by using XRD. The XRD patterns suggest that the as-synthesized compound is composed of a single hexagonal phase with a space group of P6222, which agrees well with the JCPDS No. 34-1380 standard, as shown in Figure 1.

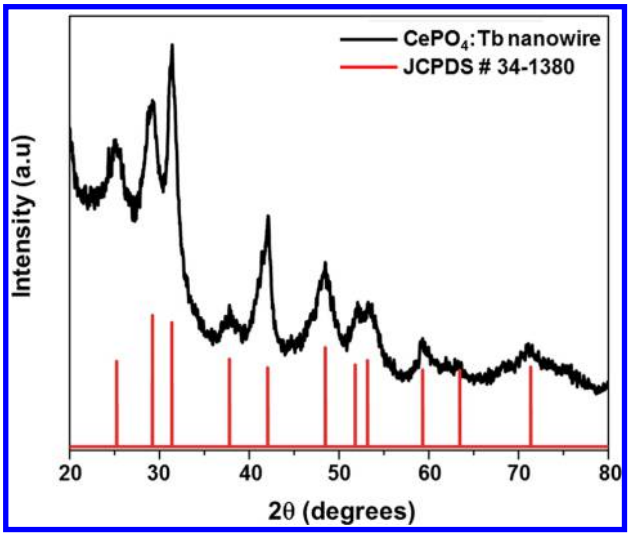

Figure 1. XRD patterns of as-prepared Tb-doped $CePO_4$ nanowires (top, black) and corresponding JCPDS No. 34-1380 database standard for bulk $CePO_4$ (bottom, red).

This hexagonal $CePO_4$ structure, which represents the prototype of lanthanum and neodymium phosphate, consists of columns built up of alternate cerium and phosphate ions, extending along the *c*-axis.[20,33−37] However, the structure contains a comparatively low density of the hexagonal isomorph, suggesting that the crystal structures can be stabilized by the presence of water at the interstices at (0, 0, $^1/_2$), (0, 0, $^5/_6$), and (0, 0, $^1/_6$), along with an open channel of the *c*-axis, as shown in Figure 2.[20] Figure 2 was prepared by using a 3D visualization program, i.e., the Visualization System for Electronic and Structural Analysis (VESTA). The presence of intercalated water molecules in the $CePO_4$ structures is easily confirmed by FTIR spectra, as illustrated in Figure S3 in the Supporting Information. The appearance of distinctive bands, associated with OH stretches and bends, in Figure S3 in the Supporting Information is typical for the hydrated form of $CePO_4$, as suggested by Hezel et al.,[35] and the water molecules

dx.doi.org/10.1021/jp4113816 | J. Phys. Chem. C 2014, 118, 5671−5682

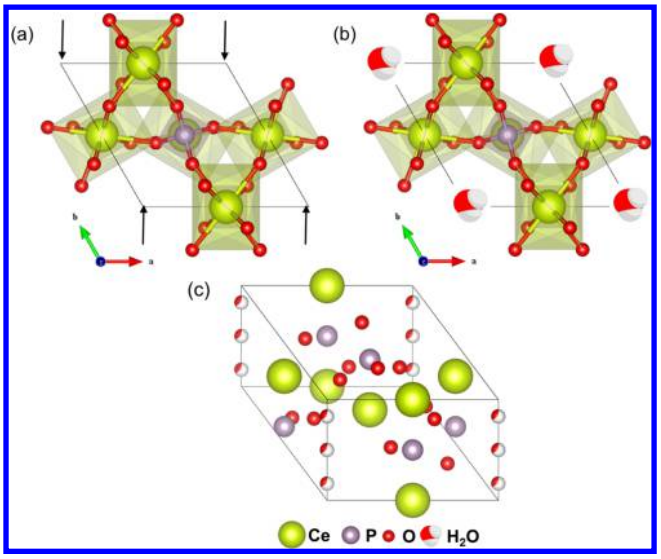

Figure 2. Unit cell representation of the crystal structure of (a) $CePO_4$ along the [001] direction and (b) hydrated $CePO_4$ along the [001] direction, as well as (c) an arbitrary direction. Arrows in part a highlight the open channels in the structures. Green, purple, and red spheres represent Ce, P, and O ions, respectively. The polyhedral geometry of CeO_6 and PO_4 is depicted by the presence of green and purple polyhedra, respectively.

are known to exist up to 800 °C in various phosphate nanoparticles.[36] We note, however, that the presence of structural water molecules of the hexagonal phosphate structure does not significantly alter their luminescent properties.[37]

2. Structural Characterization of CdSe QD−$CePO_4$:Tb Heterostructures. The size, structure, and morphology of CdSe QD−Tb-doped $CePO_4$ nanowires have been investigated by using TEM. Typical TEM images are shown in Figure 3a. Specifically, the inset in Figure 3a highlights a lower magnification image of as-prepared heterostructures. On the basis of statistical measurements of several tens of nanowires pertaining to each of our samples, our as-prepared $CePO_4$:Tb nanowires measure on average 65 ± 10 nm in diameter with lengths of up to 1.9 ± 0.47 μm.

Although the contrast variation between CdSe QDs and $CePO_4$:Tb is not dramatic under standard TEM conditions (i.e., it is somewhat difficult to differentiate between the two materials in Figure 3a), the HRTEM image (Figure 3b) of individual CdSe QD−$CePO_4$:Tb heterostructures clearly shows that highly crystalline CdSe QDs are indeed closely bound onto the underlying $CePO_4$:Tb nanowire template. The average size of the observed CdSe QDs is 4.05 ± 0.53 nm. In addition, HRTEM revealed an interlayer spacing of 0.21 and 0.31 nm in good agreement with the expected *d* spacing of the (110) and (200) lattice plane, respectively, of a hexagonal structure of CdSe QDs and $CePO_4$:Tb, respectively. The associated SAED pattern (Figure 3c) suggests that the individual features in the diffraction patterns can be assigned to either CdSe QDs or $CePO_4$:Tb nanowires.

However, quantitatively determining the spatial coverage of QDs on the $CePO_4$:Tb nanowires is not particularly straightforward to achieve simply by using standard TEM images. Thus, a detailed chemical analysis was carried out using EDS to investigate elemental composition throughout the heterostructures, so as to confirm the presence of CdSe QDs anchored onto $CePO_4$:Tb nanowires and to deduce the corresponding coverage uniformity. Specifically, scanning transmission electron microscopy images of typical nanowire segments as well as their corresponding elemental maps are highlighted in Figure 4a−f and these data shed light on the spatial distributions of the constituent elements, i.e., Ce, P, O, Cd, and Se. Interestingly, in Figure 4e and f, the locations of the Cd *L*-edge and the Se *K*-edge signals overlap reasonably well with those of the Ce *L*-edge, the O *K*-edge, and the P *K*-edge (Figure 4b−d), thereby indicating that CdSe QDs are likely attached to and spatially distributed in a uniform manner on the external surface of the $CePO_4$:Tb nanowire structure.

The surface chemical bonding structure of the heterostructures has been confirmed by FTIR spectra, as shown in Figure 5. Specifically, spectra a−c in Figure 5 highlight the FT-IR spectra of as-prepared TOPO-capped CdSe QDs, CdSe QD−$CePO_4$:Tb heterostructures, and $CePO_4$:Tb nanowires, respectively. The presence of the bands due to C−H stretching vibrations has been monitored between 2800 and 3000 cm^{-1} and the observed distinctive peak near ∼1467 cm^{-1} has been ascribed to a P═O stretching vibrational band of bound TOPO molecules on QDs in as-prepared CdSe QDs, as shown in Figure 5a.[38] Notable peaks near 3420 and 1632 cm^{-1} are likely attributed to stretching and bending vibrational modes of water molecules, and broad bands near 1064 cm^{-1} are associated with the PO_4^{3-} group in $CePO_4$ nanowire structures.[35] In CdSe QD−$CePO_4$:Tb heterostructures, the IR spectra contain a number of specific peaks, which are unambiguously altered as compared with those associated with single, individual CdSe QDs and $CePO_4$:Tb nanowire precursors. Specifically, first, the P═O stretching vibration near 1467 cm^{-1}, which represents TOPO molecules bound to

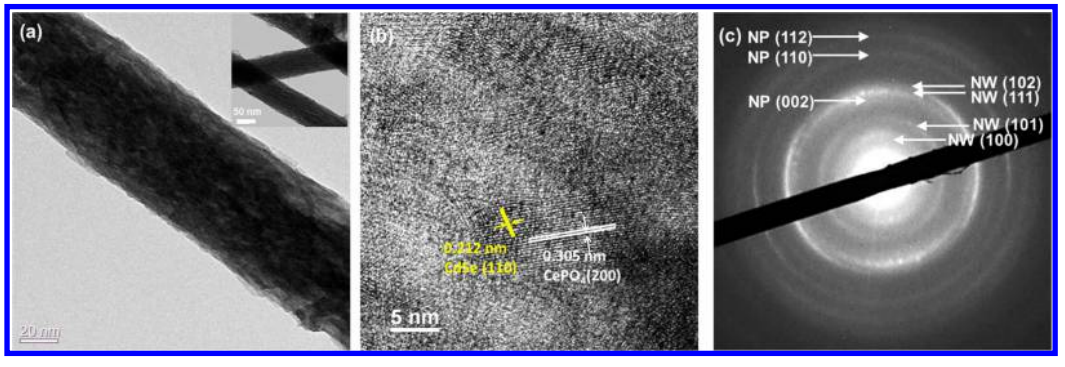

Figure 3. Representative (a) TEM, (b) HRTEM image, and (c) SAED pattern of CdSe−$CePO_4$:Tb heterostructures. NP designates CdSe particle reflections, whereas NW denotes $CePO_4$:Tb wire reflections. The inset in part a is a lower magnification image.

dx.doi.org/10.1021/jp4113816 | J. Phys. Chem. C 2014, 118, 5671−5682

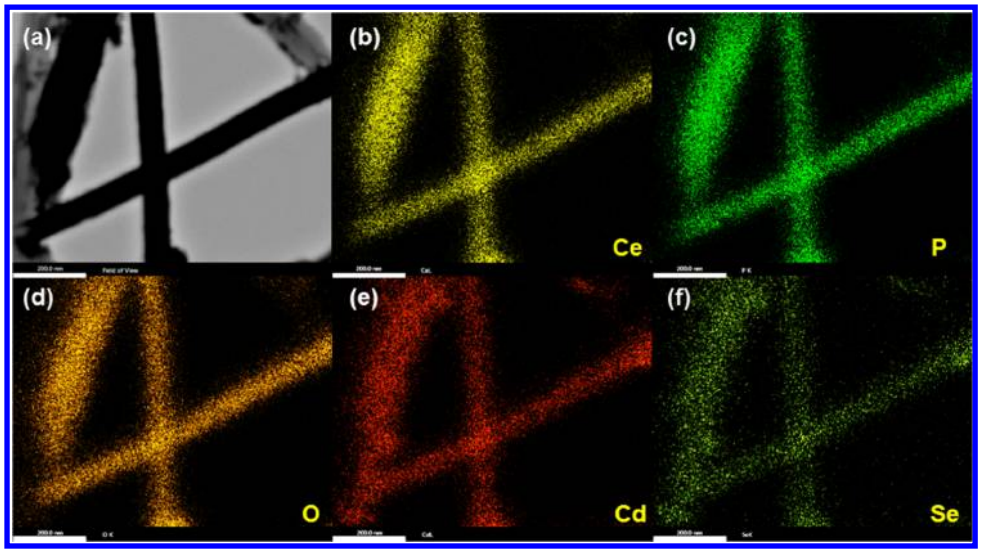

Figure 4. (a) Dark-field STEM image recorded on adjoining CdSe QD−$CePO_4$:Tb nanoscale heterostructures. (b− f) Elemental EDS mapping of the same region of nanowires, highlighting the spatial chemical distribution of Ce (bright yellow), P (green), O (dark yellow), Cd (red-brown), and Se (green-yellow), respectively. The scale bar is 200 nm in every image.

as-prepared CdSe QDs, is red-shifted to 1454 cm^{-1} (Figure 5d). Second, the O−H stretching vibration near 3420 cm^{-1} is shifted to 3450 cm^{-1} (see Figure 5e). These data imply that intermolecular hydrogen bonding (i.e., through the presence of P═O---H linkages) is likely associated with the formation of this CdSe QD−$CePO_4$:Tb nanoscale heterostructure.[39,40] We do note that the position of the O−H bending vibration near 1632 cm^{-1} is not significantly shifted in the heterostructures, since bending vibrations are normally weaker than the corresponding stretching vibrations.

3. Optical Characterization and Fluorescence Imaging. Figure 6 displays UV−visible absorption spectra of as-prepared CdSe QDs, $CePO_4$:Tb, and the resulting heterostructures. CdSe QDs and $CePO_4$:Tb nanowires exhibit well-pronounced absorption peaks at ∼550 and ∼280 nm, respectively. No significant differences in the absorbance between CdSe QDs and CdSe QD−$CePO_4$:Tb heterostructures were observed near the first excitonic absorption peak near 550 nm, suggesting that the optical density of CdSe QDs and CdSe QD−$CePO_4$:Tb is comparable, though a ∼3 nm red-shift in the peak position, perhaps due to aggregation effects, was noted for the heterostructures. The intensity of the ∼280 nm peak, which represents the pronounced absorption peak of $CePO_4$:Tb, is somewhat attenuated in the heterostructures. It is conceivable that in the heterostructure, the phosphate peak signal overlaps with and is to some extent overwhelmed by the strong intrinsic absorption of the CdSe QDs.

The steady-state photoluminescence (PL) spectra of CdSe QD−$CePO_4$:Tb heterostructures excited at 375 (3.31 eV) and 280 nm (4.43 eV) are shown in Figure 7, panels a and b, respectively. Specifically, the emission spectra of CdSe QDs consists of a high-energy peak, corresponding to a band edge emission at 568 nm without any surface trap emission in the near-infrared region, thereby indicating that CdSe QDs are likely to be uniformly and densely capped with ligands, such as TOPO and HDA.[32] The asymmetric spectral features of excitonic luminescence are likely indicative not only of the broad size distribution of CdSe QDs but also of spectral fluctuations in their microenvironment.[41]

Upon excitation at 280 nm, the obtained PL spectrum exhibits four well-resolved emission peaks attributed to $CePO_4$:Tb with the presence of excitonic CdSe QD emission near 568 nm. As shown in Figure 7b, the characteristic emission bands of Tb^{3+} at 492, 547, 589, and 623 nm can be ascribed to the *f*−*f* transitions emanating from the $^5D_4$-$^7F_6$, $^5D_4$-$^7F_5$, $^5D_4$-$^7F_4$, and $^5D_4$-$^7F_3$ levels, respectively.[36,42−45] The broad peak between 300 and 400 nm is a result of the *d*−*f* transitions of Ce^{3+}. Due to the relatively high concentration of Ce^{3+} in the nanowires, the excited state of Ce^{3+} is not completely quenched by energy transfer to Tb^{3+}.[42−44] The PL spectra of CdSe QD−$CePO_4$:Tb heterostructures display a substantially decreased CdSe emission peak. Moreover, no obvious spectral feature of $CePO_4$:Tb was noted in the PL spectrum (Figures 7a), excited at 375 nm, because the absorption intensity of $CePO_4$:Tb is significantly lower as shown in the absorption spectra in Figure 6, and hence, the signal might have potentially been below the detection limit of PL spectroscopy. Nevertheless, the heterostructures evince both spectral features of CdSe QDs and of $CePO_4$:Tb in the PL spectrum under 280-nm excitation, and consequently, we observed that the intensities of CdSe QDs and of $CePO_4$:Tb are substantially reduced in the composites themselves as compared with the constituent CdSe and $CePO_4$:Tb component building blocks.

Figure 8 highlights confocal fluorescence images of CdSe QD−$CePO_4$:Tb heterostructure composites. Images were collected at one channel corresponding to the excitonic emission behavior of CdSe QDs. Not surprisingly, the CdSe QDs by themselves evinced little if any discernible fluorescence in images obtained at 568 nm emission wavelengths (Figure 8a). For the heterostructures, the bright-field image (Figure 8b) along with the composite merged image (Figure 8c) include data collected upon excitation at 450 nm and clearly correlate the spectral overlap of the CdSe excitonic fluorescence with the spatial localization of the $CePO_4$:Tb nanowires, thereby confirming CdSe QD attachment onto the $CePO_4$:Tb nanowires.

Panels a and b of Figure 9 highlight the emission spectra collected from CdSe QD−$CePO_4$:Tb heterostructures, prepared by using varying concentration ratios of $CePO_4$:Tb to

dx.doi.org/10.1021/jp4113816 | J. Phys. Chem. C 2014, 118, 5671−5682

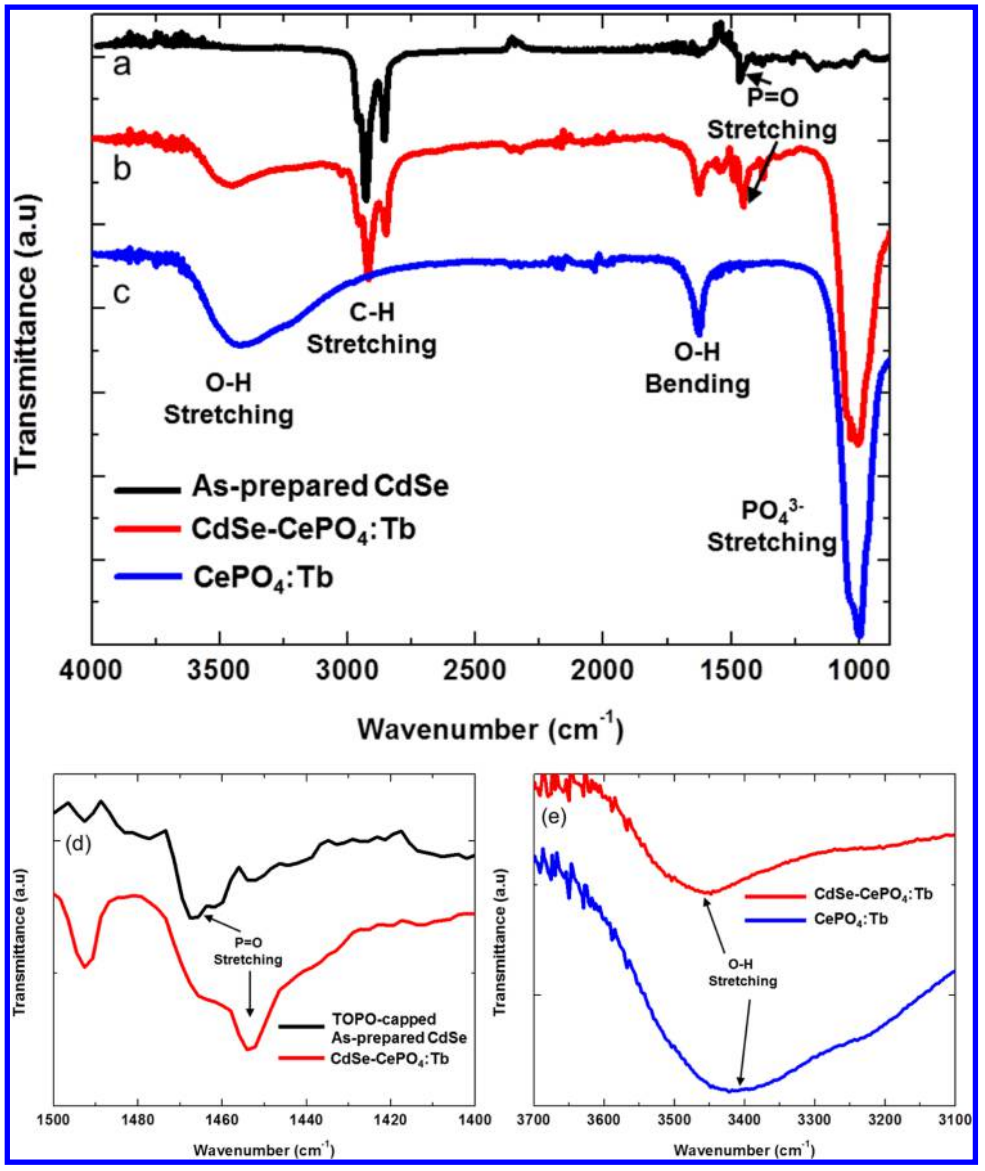

Figure 5. FT-IR spectra of (a) as-prepared, TOPO-capped CdSe QDs, (b) CdSe QD−$CePO_4$:Tb heterostructures, (c) Tb-doped $CePO_4$ nanowires, (d) as-prepared, TOPO-capped CdSe QDs and CdSe QD−$CePO_4$:Tb heterostructures in the range of the P═O stretching modes as well as (e) CdSe QD−$CePO_4$:Tb heterostructures and $CePO_4$:Tb nanowires in the range of the O−H stretching mode.

CdSe QDs and excited at 375 and 280 nm, respectively. PL quenching of the CdSe QDs was understandably more pronounced in CdSe QD−$CePO_4$:Tb heterostructures, prepared with larger quantities of CdSe QDs bound to $CePO_4$:Tb. In other words, the "free" CdSe QD emission was essentially quenched by spatial attachment onto $CePO_4$:Tb and this quenching effect increased in magnitude with correspondingly higher concentration ratios of $CePO_4$:Tb relative to CdSe QDs.

As shown in Figure S4 in the Supporting Information, at lower ratios of [$CePO_4$:Tb]/[CdSe] (i.e., in the presence of an excess of CdSe quantum dots), some of the CdSe QDs were not actually anchored onto $CePO_4$ nanowires but remained as "free" and unbound CdSe QDs. However, our data suggest that only the QDs actually attached onto the $CePO_4$:Tb nanowire itself experienced PL quenching. Therefore, since the amount of excess, free, and unbound CdSe QDs decreases with increasing nanowire surface area (i.e., with increasing concentration ratios of $CePO_4$:Tb to CdSe QDs), the PL quenching of these heterostructures became more pronounced, as all of the QDs in solution became immobilized onto "active" sites of the $CePO_4$:Tb nanowire (with an optimized effect noted with [$CePO_4$:Tb]/[CdSe] = 1). Hence, the dominant optical effect we observe in the heterostructure is that the strong CdSe emission at 568 nm tends to be reduced with greater $CePO_4$:Tb content. This distinctive trend was evident, as we systematically increased the concentration ratio of $CePO_4$:Tb to CdSe QDs from 0.33 to 1, and excited these materials at 375 and 280 nm, respectively.

To further probe the interaction between CdSe QDs and $CePO_4$:Tb, the emission decay observed with the use of a 388 nm laser pulse as the excitation source was monitored. Figure 10 illustrates the resulting excitonic emission decay of CdSe QD−$CePO_4$:Tb heterostructures. The emission decay evinced multiexponential behavior, because the distribution of the recombination rate constants associated with this complex architecture likely influenced the resulting decay kinetics.[46] Indeed, the emission intensity was analyzed using tri-exponential decay kinetics (Equation 1) in order to determine

dx.doi.org/10.1021/jp4113816 | J. Phys. Chem. C 2014, 118, 5671−5682

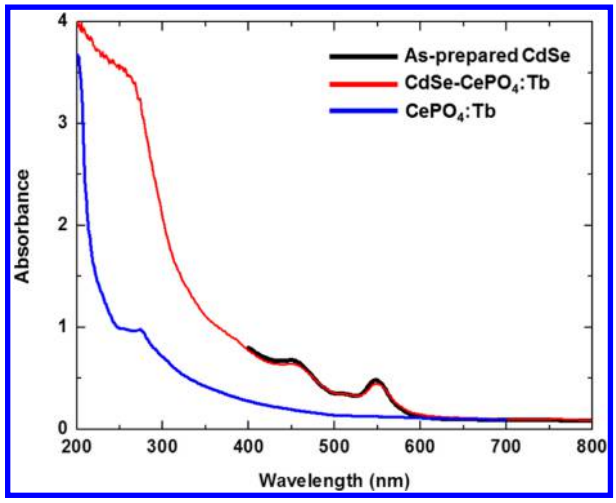

Figure 6. UV−visible spectra of as-prepared CdSe QDs, $CePO_4$:Tb nanowires, and CdSe QD−$CePO_4$:Tb heterostructures, respectively.

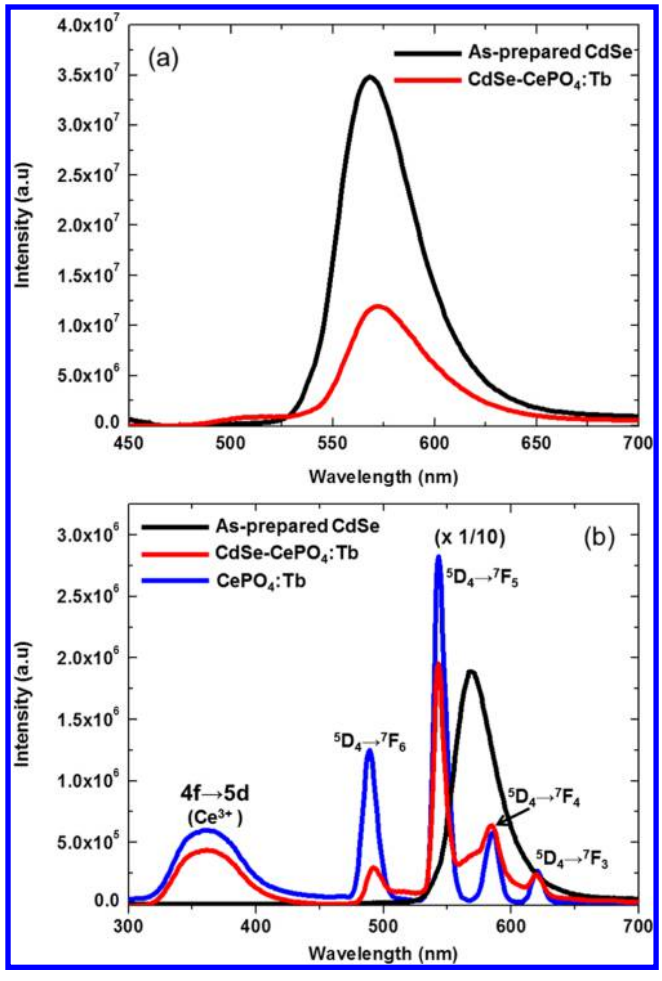

Figure 7. PL emission spectra of as-prepared CdSe QDs, $CePO_4$:Tb nanowires, and CdSe QD−$CePO_4$:Tb heterostructures, excited at (a) 375 and (b) 280 nm, respectively.

emission lifetimes (τ_i). These values were subsequently used to estimate the average lifetime (<*t*>) of the CdSe emission decay, using eq 2:[46,47]

$$F(t) = a_1 \exp\left(-\frac{t}{\tau_1}\right) + a_2 \exp\left(-\frac{t}{\tau_2}\right) + a_3 \exp\left(-\frac{t}{\tau_3}\right) \quad (1)$$

$$\langle t \rangle = \frac{\sum a_i \tau_1^{\,2}}{\sum a_i \tau_i} \quad (2)$$

The overall trends are similar for PL emission spectra. That is, the CdSe QD average lifetimes (<*t*>) decrease with increasing concentration ratios of $CePO_4$:Tb to CdSe QDs, i.e., 23.2 ns for as-prepared CdSe QDs, 22.0 ns for a ratio of 0.33, 16.9 ns for a ratio of 0.66, and 7.9 ns for a ratio of 1. The lifetimes of our as-prepared CdSe QDs are comparable with other reports of as-prepared CdSe QDs (<*t*> = 22−28 ns with a quantum efficiency ∼65%), possessing similar sizes (∼4 nm).[48,49] More detailed parameters used to obtain average lifetimes reported herein are shown in Table S1 of the Supporting Information. Substantial PL quenching and shorter lifetimes observed at higher ratios of $CePO_4$:Tb nanowires to CdSe QDs suggest that photoinduced holes in the CdSe QDs are likely transferred to the $CePO_4$:Tb nanowires under 388 nm illumination, thereby resulting in reduced PL intensities and lifetimes in CdSe QD−$CePO_4$:Tb composites as compared with the constituent components.

On the basis of all of these data, notably the obvious excitonic emission quenching and shortened lifetimes of CdSe QDs and $CePO_4$:Tb in CdSe QD−$CePO_4$:Tb nanoscale composite heterostructures, we can reasonably conclude that a photogenerated charge transfer represents the predominant relaxation pathway in CdSe QD−$CePO_4$:Tb heterostructures and that the direction of the observed charge carrier transfer is dependent upon the excitation wavelength. These observations will be discussed in detail in the next section.

4. Insights into Quenching Mechanism. To understand these experimental observations, two pathways highlighting potential external nonradiative relaxation pathways of photogenerated excitons should be considered. These include (i) resonance energy transfer of both charge carriers via a near-field electromagnetic interaction and (ii) charge transfer of one charge carrier. In our CdSe QD−$CePO_4$:Tb nanoscale heterostructures, we believe the dominant mechanism for the PL quenching and the observed shorter lifetimes is most likely due to charge transfer from CdSe QDs to $CePO_4$:Tb and vice versa and that the preferred direction of charge carrier transfer is dependent on the excitation wavelength.

As previously demonstrated by our group and others, PL quenching implies either an energy or charge transfer between two luminescent materials, and both of these processes are highly dependent upon the actual physical separation between donor and acceptor.[50−53] Indeed, we have found in QD−carbon nanotube systems that the charge transfer rate is significantly higher than the corresponding energy transfer rate at shorter lengths (i.e., <5 Å) between the two chromophores,[50] and it is well known that the energy transfer occurs when there is spectral overlap between the donor emission and the acceptor absorption.[51] In our CdSe QD−$CePO_4$:Tb heterostructures, the distance between CdSe and $CePO_4$:Tb can be estimated to be around 3.5 Å by calculating the bond length of the expected P═O---H—O bond. In effect, we did not note either an increased CdSe QD emission intensity or the appearance of new emission features in the emission spectrum of the resulting heterostructures, as shown in Figure 7.

dx.doi.org/10.1021/jp4113816 | J. Phys. Chem. C 2014, 118, 5671−5682

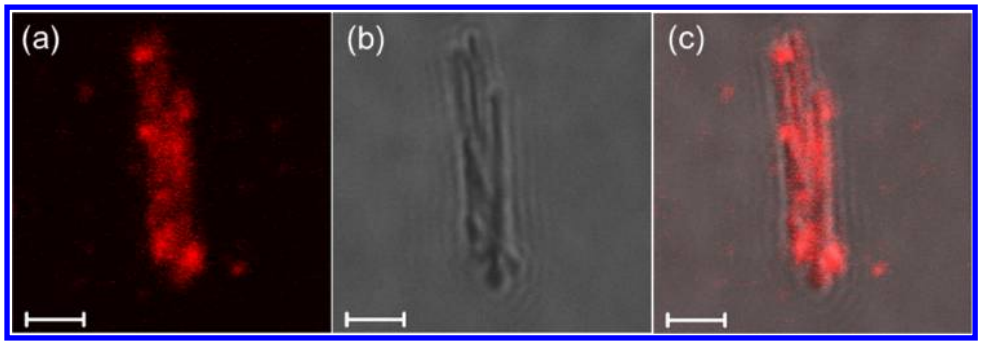

Figure 8. Confocal scanning fluorescence microscopy images of CdSe QD−$CePO_4$:Tb heterostructures collected at (a) 550 to 600 nm under 455 nm laser illumination. (b) Bright field image of CdSe QD−$CePO_4$:Tb heterostructures. (c) Composite, merged image for the CdSe QD−$CePO_4$:Tb heterostructure. Scale bars are 1 μm.

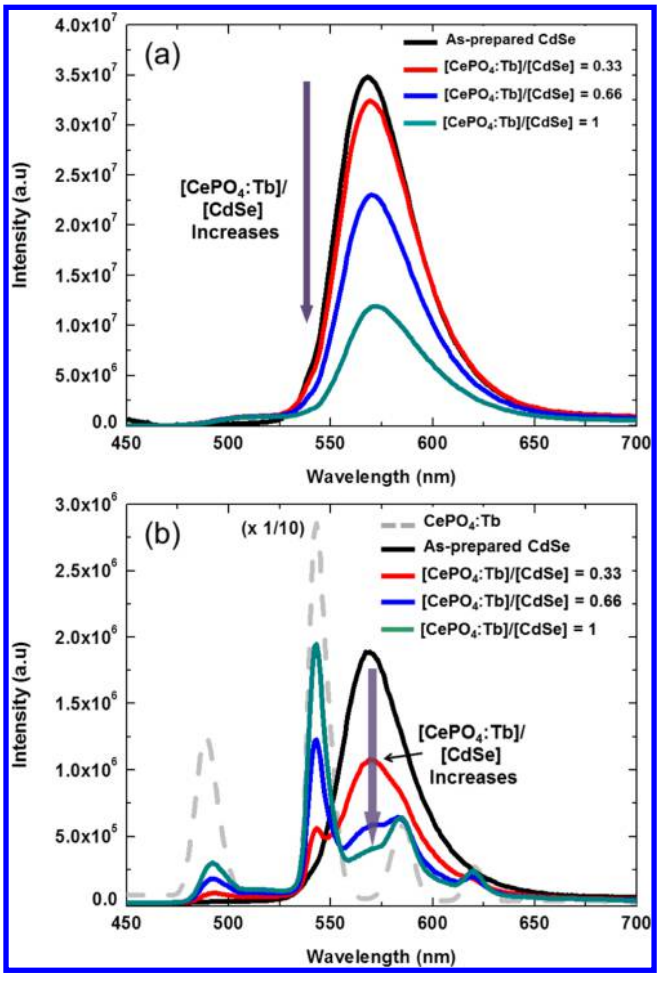

Figure 9. PL emission spectra of CdSe QD−$CePO_4$:Tb heterostructures prepared at various concentration ratios of [$CePO_4$:Tb]/[CdSe] (namely at 0.33, 0.66, and 1, respectively) and excited at (a) 375 and (b) 280 nm, respectively.

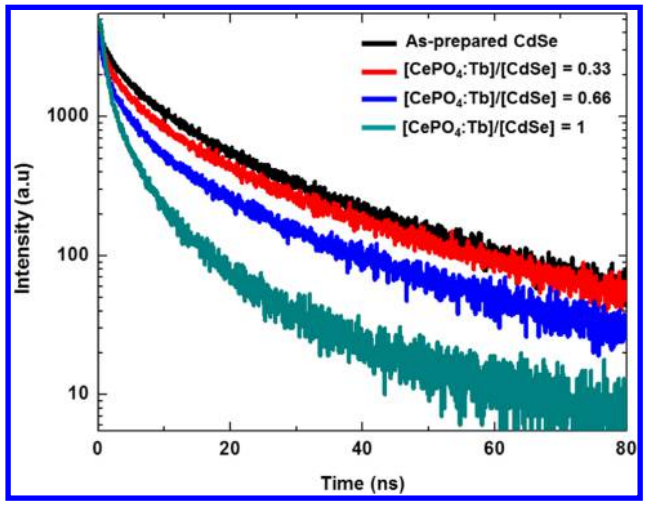

Figure 10. PL decay curves (λ_{ex} = 388 nm) of the excitonic emission of CdSe QD−$CePO_4$:Tb heterostructures prepared, from top to bottom, at increasing concentration ratios of [$CePO_4$:Tb]/[CdSe] (= 0.33, 0.66, and 1) used to synthesize these nanoscale composites.

Furthermore, Somers et al. have reported that energy transfer from luminescent materials, such as organic dyes and inorganic materials attached to QDs, is difficult to achieve when CdSe QDs act as energy transfer acceptors, since the radiative decay rate of the luminescent donor excitation energy is fast, especially as compared with the corresponding decay rate for energy transfer between the given luminescent donor and the QD acceptor.[54] Moreover, the QDs themselves can be directly excited by such excitation, thereby giving rise to potential difficulties in determining the exact extent of the energy transfer contribution to the observed QD emission.[54] In this regard, based on the known energy levels and energetics associated with our heterostructures, CdSe QDs ought to act primarily as an energy donor and the $CePO_4$:Tb nanowires should behave essentially as an energy acceptor.[53,54] In essence, the spectral overlap between the emission of QDs and the absorption of $CePO_4$:Tb should be relatively significant in order to meet the conditions necessary for energy transfer to take place. The reality is though that the spectral overlap between the emission spectra of CdSe QDs (λ_{em} = 568 nm) and the absorption spectra of $CePO_4$:Tb ($\lambda_{abs} \approx$ 280 nm) is in fact rather negligible. As such, energy transfer is likely to be a relatively unimportant process as compared with the more dominant charge transfer mechanism that would account for the PL quenching in these heterostructures.

Figure 11 shows the schematic diagram of the energy levels associated with CdSe QDs and $CePO_4$:Tb. Very recently, Dorenbos semiempirically studied and reported on the electronic level structure of various lanthanide phosphates, borates, oxides, and aluminates coupled with lanthanide activators.[55] Based on this work, it is reasonable to assume that the valence band (VB) of CdSe bulk (i.e., −6.2 eV relative to vacuum level[6]) is situated slightly below the corresponding VB of $CePO_4$:Tb (i.e., −6.1 eV). We note that the VB of CdSe

dx.doi.org/10.1021/jp4113816 | J. Phys. Chem. C 2014, 118, 5671−5682

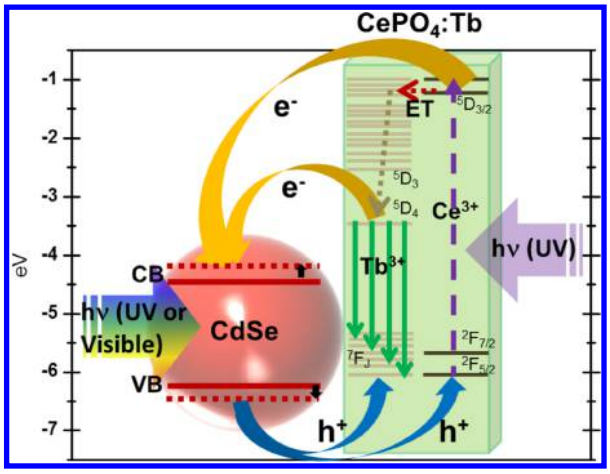

Figure 11. Electronic energy diagram of CdSe QD−$CePO_4$:Tb heterostructures and the corresponding charge transfer schematics in these materials. e^- = electron, h^+ = hole, ET = energy transfer, CB = conduction band, and VB = valence band.

QDs is substantially lower than that of CdSe bulk, due to the quantum confinement effect, and therefore speculate that there is a correspondingly larger difference between the VB of the CdSe QDs and that of $CePO_4$:Tb as compared with the corresponding VB difference between the CdSe bulk and $CePO_4$:Tb.

This situation should therefore induce the quenching of the luminescence for CdSe QDs due to hole transfer from CdSe to $CePO_4$:Tb when the CdSe QDs are optically excited, as shown in Figure 7. That is, the photoexcited holes produced upon visible illumination (i.e., 375 nm) of the VB of QDs can conceivably flow into the VB of $CePO_4$:Tb in a nonradiative fashion, prior to their recombination with photogenerated electrons in the QDs. Under deep UV irradiation (i.e., 280 nm), on the other hand, excited electrons situated in the conduction band (CB) of $CePO_4$:Tb are more likely to be transferred to the corresponding CB of CdSe QDs, thereby resulting in reduction in both Ce^{3+} and Tb^{3+} emission in the resulting heterostructures, since the CB of $CePO_4$ (i.e., −1.0 eV) lies above that of CdSe (i.e., −4.5 eV).

Even though the energy transfer from Ce^{3+} to Tb^{3+} can certainly take place within the $CePO_4$:Tb nanowire itself, the energy levels of $^5D_4$ and $^5D_3$ of Tb are still higher in energy than the CB of CdSe, and therefore, excited electrons will more favorably flow into the CB of CdSe QDs, thereby resulting in significant reduction of the PL emission of Ce^{3+} and Tb^{3+} in $CePO_4$ (i.e., ∼10 times smaller in magnitude as compared with free, underivatized $CePO_4$:Tb nanowires). In addition, the observed PL quenching of CdSe QDs can still be attributed to some extent to hole transfer from CdSe QDs to $CePO_4$:Tb nanowires. Hence, electron transfer from $CePO_4$:Tb to CdSe QDs is preferred under deep UV excitation conditions, whereas hole transfer from CdSe QDs is more pronounced upon the excitation in the range from the near-UV-to-visible region, due to the intrinsically different absorption regions of CdSe (λ_{abs} = 375−515 nm) and $CePO_4$:Tb (λ_{abs} = 250−280 nm). The implication of this work therefore is that the relaxation pathway of charge transfer between CdSe QDs and $CePO_4$:Tb can be effectively tuned by excitation wavelength. The emission peak shift at the $^5D_4$-$^7F_6$ transition as well as the different PL quenching ratios depending on the *f*−*f* transitions of Tb (e.g., the presence of PL quenching is more pronounced at lower *J* in $^5D_4$−^7F_J (*J* = 0−6) transitions) may be attributed to the presence of the midgap states of CdSe QDs, but a theoretical explanation of these phenomena is still currently under investigation.

To further confirm the presence of charge transfer from CdSe QDs to $CePO_4$:Tb, we introduced hole trapping ligands onto the surfaces of CdSe QDs in the heterostructures using a short aminothiol linker, namely AET. Specifically, both TOPO and HDA ligands were replaced with AET in a ligand exchange process (see the Experimental Section), due to the high affinity of the thiol group for the Cd surface atoms with respect to amines and TOPO. In addition, ligand exchange with thiol molecules allowed for CdSe QDs to be soluble in a wide variety of solvents (i.e., polar and apolar types). Hydrogen bonding (O−H---N) also accounted for the attachment and immobilization of AET-capped CdSe QDs onto the $CePO_4$:Tb nanowire, as mediated by amine (NH_2) groups within the AET linkers themselves.

Confocal fluorescence images of AET-capped CdSe−$CePO_4$:Tb composites confirmed that AET-capped CdSe QDs are attached to the $CePO_4$:Tb nanowires (Figure S5, Supporting Information). Similar to heterostructures synthesized with as-prepared CdSe QDs, the emission of the excitonic state of the bound AET-capped CdSe QDs to the $CePO_4$:Tb is considerably weaker than that of the "free" dots, prior to their attachment onto the $CePO_4$:Tb structural motif (Figure 12). In addition, the average lifetime of the AET-capped CdSe−$CePO_4$:Tb composite is 2.7 ns, which is considerably shorter as compared with unbound AET-capped CdSe (5.6 ns). We also note that the average lifetime of "free" AET-capped CdSe (5.6 ns) is significantly shorter than that of as-prepared CdSe (i.e., ∼23 ns), because of hole transfer associated with the AET from CdSe QDs. We have also measured the degree of PL quenching as well as lifetime values associated with AET-capped CdSe−$CePO_4$:Tb and as-prepared CdSe−$CePO_4$:Tb, wherein the as-prepared CdSe QDs were capped with TOPO and HDA, respectively. Specifically, by comparison with free, unbound CdSe QDs, the observed PL quenching of as-prepared CdSe−$CePO_4$:Tb composite and in their ligand-exchanged AET-capped CdSe−$CePO_4$:Tb composite analogues was increased by a factor of 3 and 6, respectively. The corresponding average lifetimes of as-prepared CdSe−$CePO_4$:Tb composites and of their ligand-exchanged AET-capped CdSe−$CePO_4$:Tb composite analogues decreased by a factor of 3 and 2, respectively. We should note that both heterostructures were prepared by using identical [$CePO_4$:Tb]/[CdSe] ratios.

How do we explain these observations? Because ligands play such an important role in photodynamics, it is not surprising that the excited state lifetime of AET-capped CdSe QDs (i.e., 5.6 ns) is somewhat shortened as compared with as-prepared CdSe QDs, capped with TOPO and HDA (i.e., 23 ns). Moreover, significant PL quenching and a reduced quantum yield were observed for AET-capped CdSe dots as compared with as-prepared CdSe QDs. The optoelectronic behavior of AET-capped CdSe QDs can be attributed to the presence of the "deep" trap state generated by AET ligands[56] as well as to the elimination of luminescence sites in as-prepared CdSe QDs upon binding of hole acceptors, which can lead to a more pronounced PL quenching effect but not necessarily affect observed lifetimes.[57] Furthermore, due to the partial passivation achieved by most ligands during a typical ligand exchange process,[58,59] unsaturated bonds can be present on the surfaces of AET-capped CdSe QDs, thereby giving rise to a distribution

dx.doi.org/10.1021/jp4113816 | J. Phys. Chem. C 2014, 118, 5671−5682

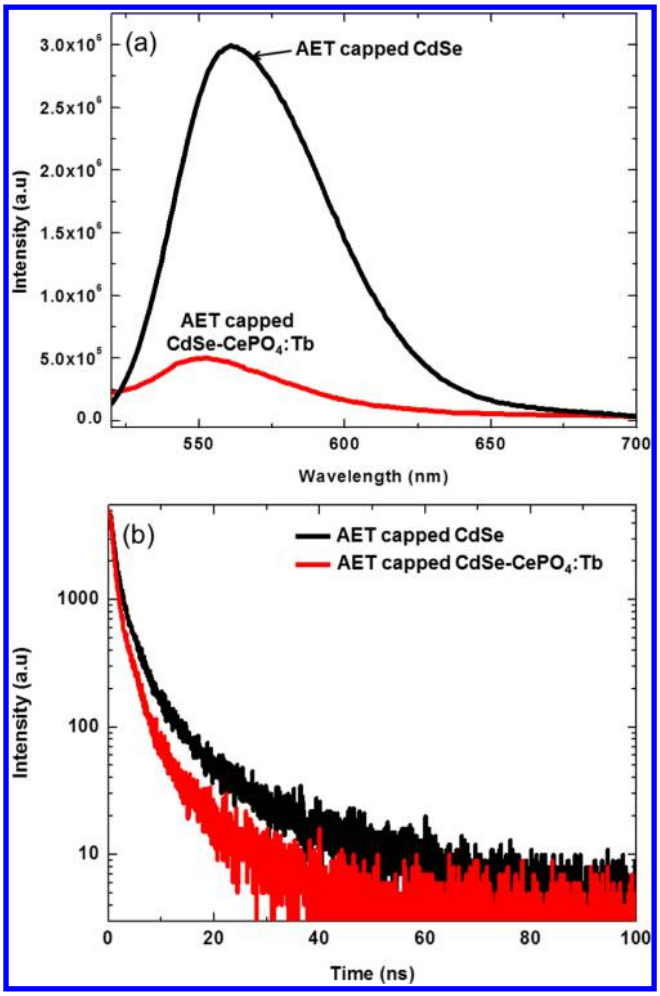

Figure 12. (a) PL emission spectra (λ_{ex} = 375 nm) and (b) emission decay curves (λ_{ex} = 388 nm) of AET-capped CdSe and AET-capped CdSe−$CePO_4$:Tb heterostructures.

of intrinsic trap sites, which can markedly diminish the inherent fluorescence emission intensity of CdSe QDs upon formation of AET-capped CdSe−$CePO_4$:Tb composites. In this sense, (a) the presence of additional surface trap states, (b) the reduced luminescence emission sites (and intensity) induced by AET molecules themselves, and (c) the formation of trap sites emanating from unsaturated bonds formed as a result of the ligand exchange process can collectively explain why the average lifetime is not as dramatically reduced as compared with the degree of PL quenching in AET-capped CdSe−$CePO_4$:Tb composites, as shown in Figure 12. A more detailed analysis to precisely deconvolute the contributions of AET surface traps from the charge transfer process occurring from the derivatized CdSe to the $CePO_4$:Tb is beyond the scope of our current study.

Nonetheless, based on all of our data, it is acceptable to infer that the PL quenching and shorter lifetimes associated with the AET-capped CdSe−$CePO_4$:Tb and the CdSe−$CePO_4$:Tb composites are affected by electron transfer from $CePO_4$:Tb to CdSe QDs as well as by hole transfer from CdSe to $CePO_4$:Tb. A similar explanation has also been noted to explain the optical behavior in CdSe−Ru−polypyridine hybrid systems, wherein PL quenching appeared in steady-state luminescence data as a result of charge transfer occurring from CdSe to Ru−polypyridine and vice versa.[60] However, it is still possible that energy transfer contributes to some extent by directly quenching a fraction of the photogenerated carriers. To determine the exact role of the QDs in the charge transfer process, femtosecond transient absorption and time-resolved PL upconversion experiments will likely be needed in future studies.

CONCLUSIONS

Preformed CdSe semiconducting 0D nanocrystals (diameter of ∼4 nm) have been successfully attached onto Tb-doped $CePO_4$ 1D nanowires, possessing very high aspect ratios (∼65 nm in diameter and ∼2 μm in length) by means of hydrogen bonding between the ligands bound to the CdSe surface and the H_2O molecules intercalated within the $CePO_4$ structure, under ambient room temperature conditions. The resulting nanoscale CdSe QD−$CePO_4$:Tb heterostructures displayed PL quenching and shorter lifetimes as compared with unbound CdSe QDs and $CePO_4$:Tb nanowires. That is, the CdSe PL quenching increased with an increased amount of attached $CePO_4$ present. That is, the effect was more pronounced with larger amounts of CdSe QDs immobilized, anchored onto, and therefore interacting with the underlying $CePO_4$:Tb nanowire motif.

The PL quenching of $CePO_4$:Tb can be attributed to photoexcited electron transfer from $CePO_4$:Tb to CdSe QDs. Moreover, the observed PL quenching and shortened average lifetimes of CdSe QDs can mainly be ascribed to photoinduced hole transfer from CdSe QDs to $CePO_4$:Tb nanowires. In particular, electron transfer from $CePO_4$:Tb to CdSe QDs is more important under deep UV excitation conditions. Conversely, hole transfer from CdSe QDs to CePO4:Tb is a more relevant process during excitation under near-UV-to-visible excitation, due to the distinctive effective absorption wavelength ranges associated with CdSe QDs and $CePO_4$:Tb. Thus, we suggest that understanding the charge transfer process in our model CdSe QD−$CePO_4$:Tb 0D nanocrystal−1D nanowire heterostructures can enable not only the ability to tune the optoelectronic properties of nanomaterials for possible incorporation into nanoscale devices but also the potential to design new types of photovoltaic architectures with the capability of effectively harvesting UV light as well as for promoting highly efficient charge separation.

ASSOCIATED CONTENT

Supporting Information

Additional structural characterization and lifetime data of the samples. This material is available free of charge via the Internet at http://pubs.acs.org.

AUTHOR INFORMATION

Corresponding Author

*E-mail: sswong@bnl.gov, stanislaus.wong@stonybrook.edu.

Notes

The authors declare no competing financial interest.

ACKNOWLEDGMENTS

Research (including support for J.K.H., L.W., and S.S.W.) was supported by the U.S. Department of Energy, Basic Energy Sciences, Materials Sciences and Engineering Division. We also acknowledge Dr. GuoWei Tian and the Central Microscopy Imaging Center (CMIC) at Stony Brook University for help with confocal microscopy measurements. Experiments were performed in part at the Center for Functional Nanomaterials

located at Brookhaven National Laboratory, which is supported by the U.S. Department of Energy under Contract No. DE-AC02-98CH10886.

REFERENCES

(1) Kong, J.; Franklin, N. R.; Zhou, C.; Chapline, M. G.; Peng, S.; Cho, K.; Dai, H. Nanotube Molecular Wires as Chemical Sensors. *Science* **2000**, *287*, 622−625.

(2) Landi, B. J.; Castro, S. L.; Ruf, H. J.; Evans, C. M.; Bailey, S. G.; Raffaelle, R. P. CdSe quantum dot-single wall carbon nanotube complexes for polymeric solar cells. *Sol. Energy Mater. Sol. Cells* **2005**, *87*, 733−746.

(3) Peng, X.; Chen, J.; Misewich, J. A.; Wong, S. S. Carbon nanotube-nanocrystal heterostructures. *Chem. Soc. Rev.* **2009**, *38*, 1076−1098.

(4) Leschkies, K. S.; Divakar, R.; Basu, J.; Enache-Pommer, E.; Boercker, J. E.; Carter, C. B.; Kortshagen, U. R.; Norris, D. J.; Aydil, E. S. Photosensitization of ZnO Nanowires with CdSe Quantum Dots for Photovoltaic Devices. *Nano Lett.* **2007**, *7*, 1793−1798.

(5) Kongkanand, A.; Tvrdy, K.; Takechi, K.; Kuno, M.; Kamat, P. V. Quantum Dot Solar Cells. Tuning Photoresponse through Size and Shape Control of CdSe−TiO_2 Architecture. *J. Am. Chem. Soc.* **2008**, *130*, 4007−4015.

(6) Robel, I.; Subramanian, V.; Kuno, M.; Kamat, P. V. Quantum Dot Solar Cells. Harvesting Light Energy with CdSe Nanocrystals Molecularly Linked to Mesoscopic TiO_2 Films. *J. Am. Chem. Soc.* **2006**, *128*, 2385−2393.

(7) Kim, D.-W.; Hwang, I.-S.; Kwon, S. J.; Kang, H.-Y.; Park, K.-S.; Choi, Y.-J.; Choi, K.-J.; Park, J.-G. Highly Conductive Coaxial SnO_2−In_2O_3 Heterostructured Nanowires for Li Ion Battery Electrodes. *Nano Lett.* **2007**, *7*, 3041−3045.

(8) Zhang, Y.; Xu, M.; Wang, F.; Song, X.; Wang, Y.; Yang, S. CuO Necklace: Controlled Synthesis of a Metal Oxide and Carbon Nanotube Heterostructure for Enhanced Lithium Storage Performance. *J. Phys. Chem. C* **2013**, *117*, 12346−12351.

(9) Yan, C.; Dadvand, A.; Rosei, F.; Perepichka, D. F. Near-IR Photoresponse in New Up-Converting CdSe/$NaYF_4$:Yb,Er Nanoheterostructures. *J. Am. Chem. Soc.* **2010**, *132*, 8868−8869.

(10) Kar, A.; Datta, A.; Patra, A. Fabrication and optical properties of core/shell CdS/$LaPO_4$:Eu nanorods. *J. Mater. Chem.* **2010**, *20*, 916−922.

(11) Kim, S.-K.; Day, R. W.; Cahoon, J. F.; Kempa, T. J.; Song, K.-D.; Park, H.-G.; Lieber, C. M. Tuning Light Absorption in Core/Shell Silicon Nanowire Photovoltaic Devices through Morphological Design. *Nano Lett.* **2012**, *12*, 4971−4976.

(12) Salant, A.; Shalom, M.; Tachan, Z.; Buhbut, S.; Zaban, A.; Banin, U. Quantum Rod-Sensitized Solar Cell: Nanocrystal Shape Effect on the Photovoltaic Properties. *Nano Lett.* **2012**, *12*, 2095−2100.

(13) McLaren, A.; Valdes-Solis, T.; Li, G.; Tsang, S. C. Shape and Size Effects of ZnO Nanocrystals on Photocatalytic Activity. *J. Am. Chem. Soc.* **2009**, *131*, 12540−12541.

(14) Borys, N. J.; Walter, M. J.; Huang, J.; Talapin, D. V.; Lupton, J. M. The Role of Particle Morphology in Interfacial Energy Transfer in CdSe/CdS Heterostructure Nanocrystals. *Science* **2010**, *330*, 1371−1374.

(15) Zheng, Y.; Gao, S.; Ying, J. Y. Synthesis and Cell-Imaging Applications of Glutathione-Capped CdTe Quantum Dots. *Adv. Mater.* **2007**, *19*, 376−380.

(16) Jang, E.; Jun, S.; Jang, H.; Lim, J.; Kim, B.; Kim, Y. White-Light-Emitting Diodes with Quantum Dot Color Converters for Display Backlights. *Adv. Mater.* **2010**, *22*, 3076−3080.

(17) Choi, J. J.; Lim, Y.-F.; Santiago-Berrios, M. E. B.; Oh, M.; Hyun, B.-R.; Sun, L.; Bartnik, A. C.; Goedhart, A.; Malliaras, G. G.; Abruña, H. c. D.; Wise, F. W.; Hanrath, T. PbSe Nanocrystal Excitonic Solar Cells. *Nano Lett.* **2009**, *9*, 3749−3755.

(18) Patra, C. R.; Bhattacharya, R.; Patra, S.; Basu, S.; Mukherjee, P.; Mukhopadhyay, D. Lanthanide Phosphate Nanorods as Inorganic Fluorescent Labels in Cell Biology Research. *Clin. Chem.* **2007**, *53*, 2029−2031.

(19) Chen, F.; Huang, P.; Zhu, Y.-J.; Wu, J.; Zhang, C.-L.; Cui, D.-X. The photoluminescence, drug delivery and imaging properties of multifunctional Eu^{3+}/Gd^{3+} dual-doped hydroxyapatite nanorods. *Biomaterials* **2011**, *32*, 9031−9039.

(20) Zhang, F.; Wong, S. S. Ambient Large-Scale Template-Mediated Synthesis of High-Aspect Ratio Single-Crystalline, Chemically Doped Rare-Earth Phosphate Nanowires for Bioimaging. *ACS Nano* **2009**, *4*, 99−112.

(21) Fang, Y.-P.; Xu, A.-W.; Dong, W.-F. Highly Improved Green Photoluminescence from $CePO_4$:Tb/$LaPO_4$ Core/Shell Nanowires. *Small* **2005**, *1*, 967−971.

(22) Maestro, P.; Huguenin, D. Industrial Applications of Rare Earths: Which Way for the End of the Century. *J. Alloys Compd.* **1995**, *225*, 520−528.

(23) Yin, Z.; Sakamoto, Y.; Yu, J.; Sun, S.; Terasaki, O.; Xu, R. Microemulsion-Based Synthesis of Titanium Phosphate Nanotubes via Amine Extraction System. *J. Am. Chem. Soc.* **2004**, *126*, 8882−8883.

(24) Xu, L.; Song, H.; Dong, B.; Wang, Y.; Bai, X.; Wang, G.; Liu, Q. Electrospinning Preparation and Photoluminescence Properties of Lanthanum Phosphate Nanowires and Nanotubes. *J. Phys. Chem. C* **2009**, *113*, 9609−9615.

(25) Huo, Z.; Chen, C.; Chu, D.; Li, H.; Li, Y. Systematic Synthesis of Lanthanide Phosphate Nanocrystals. *Chem.—Eur. J.* **2007**, *13*, 7708−7714.

(26) Yang, M.; You, H.; Liu, K.; Zheng, Y.; Guo, N.; Zhang, H. Low-Temperature Coprecipitation Synthesis and Luminescent Properties of $LaPO_4$:Ln^{3+} (Ln^{3+} = Ce^{3+}, Tb^{3+}) Nanowires and $LaPO_4$:Ce^{3+},Tb^{3+}/$LaPO_4$ Core/Shell Nanowires. *Inorg. Chem.* **2010**, *49*, 4996−5002.

(27) Li, W.; Lee, J. Microwave-Assisted Sol−Gel Synthesis and Photoluminescence Characterization of $LaPO_4$:Eu^{3+},Li^+ Nanophosphors. *J. Phys. Chem. C* **2008**, *112*, 11679−11684.

(28) Zhang, F.; Mao, Y.; Park, T. J.; Wong, S. S. Green Synthesis and Property Characterization of Single-Crystalline Perovskite Fluoride Nanorods. *Adv. Funct. Mater.* **2008**, *18*, 103−112.

(29) Zhou, H.; Wong, S. S. A Facile and Mild Synthesis of 1-D ZnO, CuO, and α-Fe_2O_3 Nanostructures and Nanostructured Arrays. *ACS Nano* **2008**, *2*, 944−958.

(30) Mao, Y.; Zhang, F.; Wong, S. S. Ambient Template-Directed Synthesis of Single-Crystalline Alkaline-Earth Metal Fluoride Nanowires. *Adv. Mater.* **2006**, *18*, 1895−1899.

(31) Mao, Y.; Wong, S. S. General, Room-Temperature Method for the Synthesis of Isolated as Well as Arrays of Single-Crystalline ABO_4-Type Nanorods. *J. Am. Chem. Soc.* **2004**, *126*, 15245−15252.

(32) Qu, L.; Peng, X. Control of Photoluminescence Properties of CdSe Nanocrystals in Growth. *J. Am. Chem. Soc.* **2002**, *124*, 2049−2055.

(33) Fang, Y.-P.; Xu, A.-W.; Song, R.-Q.; Zhang, H.-X.; You, L.-P.; Yu, J. C.; Liu, H.-Q. Systematic Synthesis and Characterization of Single-Crystal Lanthanide Orthophosphate Nanowires. *J. Am. Chem. Soc.* **2003**, *125*, 16025−16034.

(34) Mooney, R. X-ray diffraction study of cerous phosphate and related crystals. I. Hexagonal Modification. *Acta Crystallogr.* **1950**, *3*, 337−340.

(35) Hezel, A.; Ross, S. D. Forbidden Transitions in the Infrared Spectra of Tetrahedral Anions—III. Spectra-Structure Correlations in Perchlorates, Sulphates and Phosphates of the Formula MXO_4. *Spectrochim. Acta* **1966**, *22*, 1949−1961.

(36) Luwang, M. N.; Ningthoujam, R. S.; Srivastava, S. K.; Vatsa, R. K. Disappearance and Recovery of Luminescence in Bi^{3+}, Eu^{3+} Codoped YPO_4 Nanoparticles Due to the Presence of Water Molecules Up to 800 °C. *J. Am. Chem. Soc.* **2011**, *133*, 2998−3004.

(37) Buissette, V.; Moreau, M.; Gacoin, T.; Boilot, J.-P.; Chane-Ching, J.-Y.; Le Mercier, T. Colloidal Synthesis of Luminescent Rhabdophane $LaPO_4$:Ln^{3+}·xH_2O (Ln = Ce, Tb, Eu; $x \approx 0.7$) Nanocrystals. *Chem. Mater.* **2004**, *16*, 3767−3773.

(38) Sharma, S. N.; Sharma, H.; Singh, G.; Shivaprasad, S. M. Studies of Interaction of Amines with TOPO/TOP Capped CdSe Quantum Dots: Role of Crystallite Size and Oxidation Potential. *Mater. Chem. Phys.* **2008**, *110*, 471−480.

(39) Ji, S.; Jiang, T.; Xu, K.; Li, S. FTIR Study of the Adsorption of Water on Ultradispersed Diamond Powder Surface. *Appl. Surf. Sci.* **1998**, *133*, 231−238.
(40) Gramstad, T. Studies of Hydrogen Bonding—VIII. Hydrogen-Bond Association between Phenol and Sulphoxides and Nitroso Compounds. *Spectrochim. Acta* **1963**, *19*, 829−834.
(41) Resch-Genger, U.; Grabolle, M.; Cavaliere-Jaricot, S.; Nitschke, R.; Nann, T. Quantum Dots versus Organic Dyes As Fluorescent Labels. *Nat. Methods* **2008**, *5*, 763−775.
(42) Fu, Z.; Bu, W. High Efficiency Green-Luminescent $LaPO_4$:Ce,Tb Hierarchical Nanostructures: Synthesis, Characterization, and Luminescence Properties. *Solid State Sci.* **2008**, *10*, 1062−1067.
(43) Rambabu, U.; Munirathnam, N. R.; Prakash, T. L.; Buddhudu, S. Emission spectra of $LnPO_4$:RE^{3+} (Ln = La, Gd; RE = Eu, Tb and Ce) Powder Phosphors. *Mater. Chem. Phys.* **2003**, *78*, 160−169.
(44) Li, Q.; Yam, V. W.-W. Redox Luminescence Switch Based on Energy Transfer in $CePO_4$:Tb^{3+} Nanowires. *Angew. Chem., Int. Ed.* **2007**, *46*, 3486−3489.
(45) Chen, G.; Sun, S.; Zhao, W.; Xu, S.; You, T. Template Synthesis and Luminescence Properties of $CePO_4$:Tb Nanotubes. *J. Phys. Chem. C* **2008**, *112*, 20217−20221.
(46) Shimizu, K. T.; Woo, W. K.; Fisher, B. R.; Eisler, H. J.; Bawendi, M. G. Surface-Enhanced Emission from Single Semiconductor Nanocrystals. *Phys. Rev. Lett.* **2002**, *89*, 117401.
(47) James, D. R.; Liu, Y.-S.; De Mayo, P.; Ware, W. R. Distributions of Fluorescence Lifetimes: Consequences for the Photophysics of Molecules Adsorbed on Surfaces. *Chem. Phys. Lett.* **1985**, *120*, 460−465.
(48) Ebenstein, Y.; Mokari, T.; Banin, U. Fluorescence Quantum Yield of CdSe/ZnS Nanocrystals Investigated by Correlated Atomic-Force and Single-Particle Fluorescence Microscopy. *Appl. Phys. Lett.* **2002**, *80*, 4033−4035.
(49) Wuister, S. F.; de Mello Donegá, C.; Meijerink, A. Influence of Thiol Capping on the Exciton Luminescence and Decay Kinetics of CdTe and CdSe Quantum Dots. *J. Phys. Chem. B* **2004**, *108*, 17393−17397.
(50) Peng, X.; Misewich, J. A.; Wong, S. S.; Sfeir, M. Y. Efficient Charge Separation in Multidimensional Nanohybrids. *Nano Lett.* **2011**, *11*, 4562−4568.
(51) Dibbell, R. S.; Watson, D. F. Distance-Dependent Electron Transfer in Tethered Assemblies of CdS Quantum Dots and TiO_2 Nanoparticles. *J. Phys. Chem. C* **2009**, *113*, 3139−3149.
(52) Liu, B.; Gaylord, B. S.; Wang, S.; Bazan, G. C. Effect of Chromophore-Charge Distance on the Energy Transfer Properties of Water-Soluble Conjugated Oligomers. *J. Am. Chem. Soc.* **2003**, *125*, 6705−6714.
(53) Clegg, R. M.: Chapter 1 Förster Resonance Energy Transfer—FRET What Is It, Why Do It, and How It's Done. In *Laboratory Techniques in Biochemistry and Molecular Biology*; Gadella, T. W. J., Ed.; Elsevier: New York, NY, 2009; Vol. *33*; pp 1−57.
(54) Somers, R. C.; Bawendi, M. G.; Nocera, D. G. CdSe Nanocrystal Based Chem-/Bio- Sensors. *Chem. Soc. Rev.* **2007**, *36*, 579−591.
(55) Dorenbos, P. The electronic level structure of lanthanide impurities in $REPO_4$, $REBO_3$, $REAlO_3$, and RE_2O_3 (RE = La, Gd, Y, Lu, Sc) compounds. *J. Phys.: Condens. Matter* **2013**, *25*, 225501.
(56) Burda, C.; Link, S.; Mohamed, M.; El-Sayed, M. The Relaxation Pathways of CdSe Nanoparticles Monitored with Femtosecond Time-Resolution from the Visible to the IR: Assignment of the Transient Features by Carrier Quenching. *J. Phys. Chem. B* **2001**, *105*, 12286−12292.
(57) Landes, C.; Burda, C.; Braun, M.; El-Sayed, M. A. Photoluminescence of CdSe Nanoparticles in the Presence of a Hole Acceptor: n-Butylamine. *J. Phys. Chem. B* **2001**, *105*, 2981−2986.
(58) Eijt, S. W. H.; van Veen, A.; Schut, H.; Mijnarends, P. E.; Denison, A. B.; Barbiellini, B.; Bansil, A. Study of Colloidal Quantum-Dot Surfaces Using an Innovative Thin-Film Positron 2D-ACAR Method. *Nat. Mater.* **2006**, *5*, 23−26.
(59) Kalyuzhny, G.; Murray, R. W. Ligand Effects on Optical Properties of CdSe Nanocrystals. *J. Phys. Chem. B* **2005**, *109*, 7012−7021.
(60) Sykora, M.; Petruska, M. A.; Alstrum-Acevedo, J.; Bezel, I.; Meyer, T. J.; Klimov, V. I. Photoinduced Charge Transfer between CdSe Nanocrystal Quantum Dots and Ru−Polypyridine Complexes. *J. Am. Chem. Soc.* **2006**, *128*, 9984−9985.